Published in final edited form as:
Mol Cancer Ther. 2015 January ; 14(1): 3–13. doi:10.1158/1535-7163.MCT-14-0755-T.

Repurposing the antihelmintic mebendazole as a hedgehog inhibitor

Andrew R. Larsen[1], **Ren-Yuan Bai**[2], **Jon H. Chung**[1], **Alexandra Borodovsky**[2], **Charles M. Rudin**[3], **Gregory J. Riggins**[2], and **Fred Bunz**[1]

[1]Department of Radiation Oncology and Molecular Radiation Sciences, The Kimmel Cancer Center at Johns Hopkins, Baltimore, Maryland [2]Department of Neurosurgery, The Kimmel Cancer Center at Johns Hopkins, Baltimore, Maryland [3]Memorial Hospital Research Laboratories, Memorial Sloan Kettering Cancer Center, New York, NY

Abstract

The hedgehog (Hh) signaling pathway is activated in many types of cancer and therefore presents an attractive target for new anticancer agents. Here we show that mebendazole (MBZ), a benzamidazole with a long history of safe use against nematode infestations and hydatid disease, potently inhibited Hh signaling and slowed the growth of Hh-driven human medulloblastoma cells at clinically attainable concentrations. As an antiparasitic, MBZ avidly binds nematode tubulin and causes inhibition of intestinal microtubule synthesis. In human cells, MBZ suppressed the formation of the primary cilium, a microtubule-based organelle that functions as a signaling hub for Hh pathway activation. The inhibition of Hh signaling by MBZ was unaffected by mutants in the gene that encodes the Hh pathway signaling protein SMO, which are selectively propagated in cell clones that survive treatment with the Hh inhibitor vismodegib. Combination of vismodegib and MBZ resulted in additive Hh signaling inhibition. Because MBZ can be safely administered to adults and children at high doses over extended time periods, we propose that MBZ could be rapidly repurposed and clinically tested as a prospective therapeutic agent for many tumors that are dependent on Hh signaling.

Keywords

benzimidazole; hedgehog; smoothened; primary cilium; brain tumors

Corresponding authors: Fred Bunz, 1550 Orleans Street, Room 453, Baltimore, Maryland 21287. Phone 410-502-7941; Fax 410-502-2821; fbunz@jhmi.edu. Gregory J. Riggins, 1550 Orleans Street, Room 257, Baltimore, Maryland 21287; Phone 410-614-0477; Fax 410-614-0478; griggin1@jhmi.edu.

Potential conflicts of interest: None.

Author contributions:
Conception and design: A.R. Larsen, G. Riggins, F. Bunz
Acquisition of data: A.R. Larsen
Analysis and interpretation of data: A.R. Larsen, F. Bunz
Writing review and/or revision of the manuscript: A.R. Larsen, G. Riggins, F. Bunz
Administrative, technical or material support: R-Y Bai, J.H. Chung, A. Borodovsky
Study supervision: G.J. Riggins, F. Bunz

Introduction

Activation of the hedgehog (Hh) signaling pathway is required for developmental morphogenesis and is frequently observed in human cancers (1,2). Canonical Hh signals are initiated by the interaction of Hh ligands with the receptor PTCH1. In the unbound state, PTCH1 prevents SMO activation in the primary cilium, an organelle required for the transduction of various chemical and mechanical signals (3). In the presence of ligand, PTCH1 disappears from the cilium and SMO activates downstream effectors, including the GLI family of transcription factors (4). Several types of cancer, including basal cell carcinoma and medulloblastoma, are frequently caused by germline or somatic mutations in *PTCH1* or by less common alterations within the pathway that lead to constitutive signaling by SMO (1,2). Alternative modes of Hh pathway activation in some of the most common types of cancer are suggested by the widespread presence of Hh ligands and evidence of elevated GLI activity in many tumors that lack pathway-activating mutations (5,6).

SMO antagonism has proven to be an effective strategy for treating tumors with active Hh signaling (7). The first SMO antagonist to be approved for clinical use is vismodegib (Erivedge, also known as GDC-0449). Vismodegib has been used successfully for the treatment of locally advanced and metastatic basal cell carcinomas (8), and is currently being tested for use in adults and children with many diverse types of tumors, including medulloblastomas and gliomas, which are often refractory to conventional therapies (9). When used as a monotherapy, vismodegib is associated with adverse effects that include fatigue, vomiting, weight loss, decreased appetite, dysgeusia, dehydration, and muscle spasm (10). Such low-grade toxicities have contributed to treatment discontinuation and appear to be potentially problematic when vismodegib is combined with conventional agents (11). When used to treat a patient with metastatic medulloblastoma, vismodegib caused a response that was impressive but transient (12). Recurrent tumors in this patient were found to harbor a novel *SMO* mutation that caused drug resistance (13). Selection for *SMO*-mutant tumor cell populations can similarly be caused by vismodegib therapy in mouse models of medulloblastoma (13). Alternative strategies to inhibit Hh signaling have been explored for the prevention or treatment of such recurrent tumors (14).

Benzimidazoles approved by the US Food and Drug Administration for the treatment of nematode infections have been reported to have antiproliferative effects in diverse types of cancer cells, including those derived from melanoma, non-small cell lung cancer, ovarian cancer, adrenocortical carcinoma, and colorectal cancers (15–20). Case reports have documented responses of a metastatic adrenocortical carcinoma (21) and a metastatic colorectal carcinoma (22) to mebendazole (methyl N-[6-(benzoly)-1H-benzamidazol-2-yl] carbamate; MBZ). Our group recently found that experimental brain tumors were highly sensitive to benzimidazole therapy that was administered to a mouse colony for control of a pinworm infestation. Follow up studies of this serendipitous observation showed that mebendazole inhibited the growth of glioma-derived neurospheres *in vitro*, and among the benzimidazoles most effectively entered the central nervous system and slowed the growth of orthotopically implanted gliomas, which are characteristically resistant to standard modes of therapy (23).

The anticancer effect of MBZ defies a simple explanation. MBZ and related compounds have been reported to cause growth arrest and induce apoptosis in cultured cancer cells at doses that have little effect on non-cancer immortalized cells (15–17,19,20). It is unclear why such nonspecific antiproliferative effects would preferentially target tumor cells over the cells in normal renewing tissues. Like all benzimidazoles used for treatment of helminth infestations, MBZ binds tubulin at a binding site also recognized by colchicine, and inhibits microtubule polymerization. The rate of dissociation of MBZ from nematode tubulin is an order of magnitude lower than from human tubulin (24). Inhibition of microtubule formation in the gut of the nematode prevents the absorption of glucose and thereby leads to elimination of the parasite (25), whereas human cells and tissues are apparently minimally affected by the less avid MBZ-tubulin interaction. MBZ is therefore well tolerated, even at high doses administered over lengthy time periods for treatment of cystic echinococcosis (26).

A growing body of evidence suggests that activated Hh signaling contributes to the diverse cancers that are pre-clinically responsive to MBZ and structurally related benzimidazoles. Recently, Hh signaling has been shown to be active in many gliomas (27,28), while Hh ligands or markers of downstream pathway activity have been detected in melanomas, lung cancers, ovarian cancers, adrenocortical cancers and colorectal cancers (5,6,29–32), which are all responsive to MBZ (15–21). Notably, unbiased screens for novel Hh inhibitors have previously identified drugs that interact with microtubules, including vinblastine, vincristine, and paclitaxel (33). These drugs potently inhibit mitosis, are highly toxic and therefore unsuitable for long term therapy. The specific effects of these compounds on components of the Hh pathway have not been reported.

In this study, we evaluated the effect of MBZ on the Hh pathway. MBZ treatment prevented the formation of the primary cilium, decreased expression of downstream Hh pathway effectors, and decreased the proliferation and survival of human medulloblastoma cells with constitutive Hh activation. MBZ inhibited the activation of SMO mutant proteins that give rise to disease recurrence. A combination of MBZ and vismodegib achieved additive inhibition of canonical Hh signaling. These results support the repurposing of MBZ for use in the many types of cancers that are initiated or maintained by active Hh signaling, and suggest combinations of drugs that could facilitate the achievement of durable responses.

Materials and Methods

Cell lines and cell cultures

Cultures of 293T and hTERT-RPE1 cells and *Smo*−/− mouse embryo fibroblasts (MEFs) were maintained in DMEM (Life Technologies) supplemented with 10% fetal bovine serum (FBS; Hyclone) and penicillin/streptomycin. DAOY and C3H10T1/2 mouse fibroblast cells were grown in Eagle's MEM (Life Technologies) supplemented with 10% FBS and penicillin/streptomycin. NIH3T3 cells were grown in DMEM supplemented with 10% calf serum. Shh Light II cells (34) were grown in DMEM with 10% calf serum and 0.4 mg/ml geneticin and 0.15 mg/ml zeocin, both purchased from Life Technologies. All cell lines were obtained from ATCC within six months of the beginning of the project and validated

by the supplier, except for *Smo*−/− mouse embryo fibroblasts which were a gift from James Kim and were not genetically authenticated upon their receipt in July 2013.

Orthotopic tumors

Syngeneic GL261 glioma tumors were grown intracranially in 4–6 week old female *nu/nu* athymic mice (NCI-Fredrick) and treated with MBZ as previously described (23). Each brain was snap frozen after extraction and stored in liquid nitrogen until further analysis. Orthotopic medulloblastoma xenografts were generated in female athymic mice, 5–6 weeks of age (NCI). DAOY cells were infected with a lentivirus carrying a firefly luciferase cDNA (23) prior to implantation. For the implantation procedure, mice were anesthetized and 200,000 DAOY cells were injected through a burr hole drilled 1 mm lateral to the right of the sagittal suture and 1 mm posterior to the lambda at a depth of 2.5 mm below the dura, with the guidance of a stereotactic frame, at a rate of 1 μl/minute. Treatment was initiated at 5 days post implantation, with a daily dose of MBZ of 25 mg/kg or 50 mg/kg delivered with 50% (v/v) sesame oil and PBS, by gavage. Intracranial luciferase activity was determined with a bioluminescence imager (Xenogen) following intraperitoneal injection of 2 mg D-luciferin potassium salt (Gold Biotechnology). Animals were scanned 15 m after injection for 1 m at a distance of 20 cm. Mice were euthanized when they exhibited signs of increased intracranial pressure. All animal protocols and procedures were performed under an approved protocol and in accordance with the Johns Hopkins Animal Care and Use Committee guidelines. For RNA preparation, each brain was thawed on ice before removing the right anterior cerebral cortex and the contralateral brain section. Each tissue sample was suspended in 1 mL of TRIzol (Life Technologies) per 0.1 g of material, and the RNA fraction was purified according to the manufacturer's recommendations.

Plasmids and cell transfections

ShhN-conditioned media was generated by transfection of pcDNA3 ShhN (provided by Pao Tien Chuang) into 293T cells. Control media was obtained from mock-transfected 293T cells. For localization of SMO, hTERT RPE-1 cells grown in chamber slides (Nunc) were transfected with pcDNA3 Smo-FLAG (provided by Chen Ming Fan). GLI1 reporter assays were conducted by cotransfecting the firefly luciferase reporter pBV Luc 8xGli (provided by Craig Peacock) and TK-renilla luciferase reporter pGL4 74 (Promega). Overexpression of Hh components was achieved by transient transfection of pRK-SmoM2 (35), pCMV5 hGLI1 FLAG (provided by Peter Zaphiropoulos) and pCS2-MT hGLI2 FL (Addgene plasmid 17648 ref (36)). Mutant-*Smo* expression constructs were provided by James Kim. All transfections were performed with FuGENE HD (Promega).

GLI-reporter assays and drug treatment

Subconfluent Shh Light II cells were routinely incubated in low serum conditions (0.25% fetal bovine serum, 5 mm HEPES), to optimize Hh responsiveness, during a 48 h period of drug treatment. For ShhN ligand stimulation, cells were incubated with ShhN-conditioned media or control media, diluted 1:5, during the treatment period. Final DMSO concentration in all cultures was 1%. For experiments involving overexpression of Hh pathway components, cells were transfected 24 h prior to low serum and drug treatment. Cell lysates

were analyzed using the Dual Luciferase Assay Reporter System (Promega). GLI-dependent luciferase was measured on a Victor3 V 1420 Multilabel Counter (Perkin Elmer) and standardized against *renilla* luciferase activity. The IC_{50} was calculated by Prism 5 software package (GraphPad).

Cell proliferation, viability and survival assays

BrdU incorporation during DNA synthesis was measured using the Cell Proliferation ELISA kit (Roche). Cell viability was measured with the Cell Titer-Blue Cell Viability Assay kit (Promega). Colorimetric signals were measured on a SpectraMax M5 (Molecular Devices). For each assay, the IC_{50} was calculated with the Prism 5 software package (GraphPad). For assessment of clonogenic survival, cells were drug-treated under low serum conditions in 12 well plates. After 48 h, cells were harvested in trypsin-EDTA (Life Technologies), diluted 1:4000 in standard growth media and seeded in 10 cm plates, in triplicate. After 10 days of growth, plates were stained with 0.2% crystal violet in 50% MeOH and destained in water. Colonies containing more than 50 cells were scored. For the quantitation of apoptosis, cells were detached and stained with a fluorescent antibody directed against Annexin V with the Dead Cell Apoptosis Kit (Life Technologies). The fraction of stained cells was determined with a FACSAria II flow cytometer (BD) in the Sidney Kimmel Comprehensive Cancer Center Flow Cytometry Core.

Immunoblots and immunofluorescence

Proteins were separated on Bis-Tris gels (Life Technologies) and transferred onto Immobilion-P nylon membranes (Millipore). Following overnight incubation with primary antibodies under standard conditions, blots were developed with HRP-conjugated secondary antibodies and visualized by chemiluminescence (Amersham). Band intensities were quantified by Image Lab software and standardized to the intensity of the loading controls anti-α-tubulin or anti-β-actin. To assess tubulin polymerization, polymerized and unpolymerized tubulin fractions were separated on the basis of solubility as reported previously (37).

For analysis of primary cilia by immunofluorescence, cells were grown on poly-D-lysine (Sigma) coated chamber slides (Nunc) and fixed in 0.4% paraformaldehye at 37°C for 5 min, permeabilized in 0.5% Triton X-100 at 37°C for 2 min, washed in PBS, then sequentially incubated in 4% paraformaldehyde, 37°C for 5 min, and methanol, −20°C for 5 min, as previously described (38). Nonspecific proteins were blocked with 2% bovine serum albumin in PBS for 30 min at RT. Slides were incubated with primary antibody in blocking buffer overnight at 4°C, then washed with PBS and incubated with either biotinylated (Santa Cruz Biotechnology) or Alexa Fluor 594-conjugated (Life Technologies) secondary antibodies in blocking buffer for 20 min at room temperature. Cells were washed with PBS before adding an Alexa Fluor 488-streptavidin conjugate (Life Technologies). Nuclei were counterstained with 4′,6-diamidino-2-phenylindole (DAPI; Life Technologies). Stained cells were visualized with an AxioImager Z1 (Carl Zeiss) and images were captured with Axiovision Rel 4.6 software.

The following primary antibodies were used: anti-GLI1 (C68H3; Cell Signaling), anti-Caspase 3 (9662, Cell Signaling) anti-cleaved caspase 3 (D175; Cell Signaling), anti-α-tubulin (TU-02; Santa Cruz), HRP-conjugated anti-β-actin (Santa Cruz), anti-acetylated α-tubulin (6-11 B-1; Sigma), anti-FLAG (anti-DYKDDDDK; Cell Signaling).

Quantitative real time RT-PCR

RNA was isolated and purified with the TRIzol reagent (Life Technologies), treated with DNase I (Thermo Scientific) and assayed by spectrophotometry. cDNA was synthesized with the Maxima First Strand cDNA synthesis kit (Thermo Scientific). Quantitative, real time reverse-transcription PCR (qRT-PCR) was performed using both Maxima Probe and Maxima SYBR Green qPCR Master Mixes (Thermo Scientific) with standard cycling conditions on a 7900HT Fast Real-Time PCR system (Applied Biosystems). Prime Time qPCR probes and primers were used to assay the mouse genes: *Ptch1*: probe (5′-ATTCGGACCCTGCAAGCATCAGT-3′), forward primer (5′-TGTTTGCTCCCGTTCTGG-3′), reverse primer (5′-AACCAGTCCATTGAGAACCC-3′); *Gli1*: probe (5′-CTGGGACCCTGACATAAAGTTGGCT-3′); forward primer (5′-CTTTCTGGTCTGCCCTTTTG-3′); reverse primer (5′-TCTTTGTTAATTTGACTGAACTCCG-3′); *Rpl19*: probe (5′-CTTCTCAGGAGATACCGGGAATCCAAG-3′); forward primer (5′-AGAAGGTGACCTGGATGAGAA-3′); reverse primer (5′-TGATACATATGGCGGTCAATCT-3′). Human transcripts were analyzed with SYBR green. *GLI1*: forward primer (5′-CCACGGGGAGCGGAAGGAG-3′); reverse primer (5′-ACTGGCATTGCTGAAGGCTTTACTG-3′). *PTCH1*: forward primer (5′-CCACAGAAGCGCTCCTACA-3′); reverse primer (5′-CTGTAATTTCGCCCCTTCC-3′). *PTCH2*: forward primer (5′-GGAATGATTGAGCGGATGATTGA-3′); reverse primer (5′-CCACCTGTGCCTTGTCTAGC-3′). *GAPDH*: forward primer (5′-CGGAGTCAACGGATTTGGTCGTAT-3′); reverse primer (5′-AGCCTTCTCCATGGTGGTGAAGAC-3′). All results were analyzed using SDS RQ Manager (Applied Biosystems).

Results

Inhibition of Hh signaling in vitro and in vivo

To directly assess the effect of MBZ on canonical Hh signaling, we incubated the drug with murine Shh-Light II cells, which have stably incorporated a GLI-activated firefly luciferase (Gli-luc) reporter construct (34). Under low serum conditions that are optimal for Hh activation, addition of the amino-terminal signaling domain of the secreted Sonic Hedgehog ligand (ShhN) induced robust reporter activity that could be inhibited by MBZ in the micromolar dose range (Fig. 1A). A similar degree of inhibition was observed in mouse C3H10T1/2 fibroblast cells transiently transfected with the Gli-luc reporter (Fig. 1B). MBZ was a considerably more potent inhibitor of Hh pathway activation than structurally related antihelmintic drugs (Fig. 1C), which in prior studies were less effective than MBZ at inhibiting the growth of GL261 gliomas (23). The GL261 mouse tumor harbors a mutation in *Pten* (39); in humans, mutation of *PTEN* defines a category of gliomas that are strongly associated with elevated Hh activity (28). We assessed endogenous *Gli1* transcript levels in

MBZ-treated and control GL261 tumors. *Gli1* expression was significantly elevated in untreated tumors compared with non-affected tissue from the contralateral side of the brain (Fig. 1D), suggesting a role for Hh signaling in the growth of these tumors. *Gli1* transcript and protein expression in tumor tissues was decreased by MBZ treatment (Fig. 1E & F).

To extend our analysis to human cells, we tested the effects of MBZ on Hh-mediated gene expression in the immortalized human retinal pigment epithelial cell line hTERT-RPE1. Unlike the majority of human cancer cell lines, this non-cancer cell line is responsive to ShhN (Fig. 1G). A concentration of 0.1 μM MBZ was sufficient to reduce ShhN-induced expression of endogenous *GLI1* and *PTCH1* to basal levels (Fig. 1G). Further Hh pathway inhibition was observed at higher MBZ concentrations. Using the same conditions, we assessed the effect of MBZ on the human medulloblastoma cell line DAOY. In both the presence and absence of ShhN ligand there was partial reduction in *GLI1* and *PTCH1* transcripts at 0.1 μM MBZ and almost complete suppression at 1 μM MBZ, similar to the effect of 0.2 μM vismodegib (Fig. 1H).

Inhibition of Hh-dependent cell proliferation and survival, and tumor growth

We next assessed the effects of MBZ on Hh-dependent cell proliferation and survival. DAOY cells have a gene expression profile consistent with a type 2 (Hh-subtype) medulloblastoma and accordingly exhibit elevated Hh signaling (40). In these cells, MBZ caused a reduction in *GLI1* expression with an IC_{50}=516 ±81 nM (SEM; Fig. 2A). At similar concentrations MBZ markedly inhibited DAOY cell proliferation (Fig. 2B). Clonogenic survival was affected by MBZ at a concentration as low as 100 nM (Fig. 2C). The viability of DAOY cells, as assessed by a metabolic assay, was significantly impaired by MBZ at concentrations approaching 1 μM. In contrast, hTERT RPE-1 cells, which are Hh-responsive but not dependent on Hh signals for growth, were only modestly affected by this treatment (Fig. 2D). The expression of GLI1 protein was similarly reduced in both cell types by increasing concentrations of MBZ, but only DAOY cells exhibited biochemical (Fig. 2E) and morphological (Fig. 2F) evidence of apoptosis. Accordingly, a significant proportion of DAOY cells stained with Annexin V after MBZ treatment (Fig. 2G), and this response was dose dependent (Fig. 2H).

When injected into the cerebella of nude mice to form orthotopic xenograft tumors, DAOY cells were responsive to 50 mg/kg MBZ administered by daily gavage. MBZ treatment extended the median survival of tumor-bearing mice by 38 d (Fig. 3A). Levels of *GLI1* and *PTCH2* transcripts were reduced in the DAOY-derived tumors at the time of death (Fig. 3B), while bioluminescence imaging demonstrated a marked effect on tumor cell proliferation in asymptomatic mice (Fig. 3C). Treatment of mice harboring DAOY-derived orthotopic tumors with 25 mg/kg MBZ caused an increased median survival of 19 d (Fig. S1A) and similarly reduced tumor-specific expression of *GLI1* and *PTCH1* (Fig. S1B). Notably, DAOY xenografts exhibit large cell morphology (40), which in naturally-evolving tumors is associated with poor outcomes (41).

Inhibition of SMO via suppression of ciliogenesis

We next tested the ability of MBZ to counteract Hh signaling induced by individual components of the pathway. NIH3T3 cells strongly activated the Gli-luc reporter in response to ShhN-conditioned medium; this upregulation of Hh activity was suppressed by MBZ and by vismodegib (Fig. 4A). Hh signaling could also be strongly stimulated in these cells by transient overexpression of the Ptch1-resistant SmoM2 mutant protein (35), and by GLI1 or GLI2 (Fig. 4B). The stimulatory effect of SmoM2 on Gli-luc activation could be suppressed by MBZ, whereas reporter activation by the downstream effectors GLI1 and GLI2 was resistant to MBZ (Fig. 4C).

To assess the effect of MBZ on upstream signaling by SMO, we examined the cellular localization of a Smo-FLAG fusion protein (42) by immunofluorescence. Under low serum conditions that favor primary cilium formation and robust SMO activation, Smo-FLAG was predominantly localized to the primary cilia (Fig. 5A). MBZ-treated cells exhibited a notable paucity of primary cilia, and in non-ciliated cells Smo-FLAG was distributed throughout the cytoplasm (Fig. 5A). The suppressive effect of MBZ on ciliogenesis was quantified in larger cell populations (Fig. 5B and C). The proportion of ciliated cells decreased in response to MBZ within a concentration range that also inhibited the polymerization of human α-tubulin *in vitro* (Fig. 5D). We next tested whether allowing primary cilia to pre-form prior to MBZ addition could alter the effect of MBZ on pathway activity. Temporally separating serum starvation from MBZ administration partially restored *GLI1* expression (Fig. 5E) and viability (Fig. 5F) in MBZ-sensitive DAOY cells.

Distinct modes of Hh-pathway inhibition by vismodegib and MBZ

As MBZ exerts an indirect effect on SMO, we reasoned that MBZ might inhibit the activity of mutant SMO proteins that have been found to confer vismodegib resistance. To test this idea, we assayed the ability of MBZ to inhibit Gli-luc activation by wild type and vismodegib-resistant mutant Smo proteins exogenously expressed in $Smo^{-/-}$ mouse embryo fibroblasts. Gli-luc activity was induced by ShhH ligand in the presence of either wild type *Smo* or the *Smo* D477G mutant. This mutation was originally found in a vismodegib-resistant allograft derived from a mouse medulloblastoma and corresponds to an equivalent mutation found in a patient with recurrent disease (13). Activation of Gli-luc by *Smo* D477G was completely resistant to inhibition by vismodegib (Fig. 6A). In contrast, both wild type and mutant Smo could be functionally suppressed by MBZ (Fig. 6B). Analysis of an expanded panel of all described vismodegib-resistant *Smo* mutants (14) confirmed that the inhibitory effects of MBZ were unaffected by the vismodegib-selected alterations in Smo (Fig. 6C). When used in combination, vismodegib and MBZ additively suppressed the Gli-luc signal (Figs. 6D, E), a result that is consistent with two independent modes of pathway inhibition.

Discussion

The development of new drugs for the treatment of cancers is a time consuming and expensive process. Unanticipated toxicities at all stages of development are a major cause of failure (43). Repurposing well characterized compounds for new uses can minimize such

uncertainty, save time and markedly reduce costs. There are over 4000 unique molecular entities approved worldwide for human or veterinary use (44). Exploring new indications for this rich compound library is a particularly attractive strategy to find new treatments for rare and neglected diseases, for which there are few financial incentives to justify the traditional process of commercial drug discovery. Brain tumors are relatively rare, but highly lethal. The incidence of medulloblastoma, for example, is approximately 1.5 per million in the US and the majority of these cases occur in children (45). Economic constraints and the unique vulnerability of pediatric patients are obstacles to the traditional drug discovery process. New strategies to treat such diseases will likely involve agents that are first approved for other purposes.

MBZ was developed in 1968 for use against a broad spectrum of gastrointestinal helminth pathogens, and remains among the most widely used agents in infected adults, including pregnant women and children (46). Doses as high as 200 mg/kg/day have been safely and effectively administered for up to 48 weeks for the treatment of internal hydatid cysts (47,48). While systemic absorption is low, serum levels of MBZ peak one to three h after intake, at reported levels that range from 0.3– 1.6 μM (48,49). We observed significant levels of Hh pathway inhibition within this dose range. The only significant side effect of these high, chronic doses is bone marrow suppression, which has been observed in fewer than 5% of patients. Case reports suggest that this adverse effect is associated with increased therapeutic effect, and is therefore probably caused by higher blood levels of MBZ in these patients. In supportive clinical settings, this untoward effect could be straightforwardly monitored and was reversible upon cessation of treatment (50).

We show here that the low-avidity binding of MBZ to human tubulin can inhibit the assembly of the primary cilium, a tubulin-based structure. Hh pathway components are concentrated in the primary cilium (4,51), and mutations in murine genes necessary for cilium formation cause phenotypes consistent with deficiencies in Hh signaling (52). In mice, primary cilia are dispensable for the growth of fibroblasts and other cell types, but essential for the ongoing proliferation of cultured medulloblastoma cells and the growth of established tumors (53). The differences in MBZ sensitivity that we observed between human medulloblastoma cells and immortalized cells (Fig. 2D, E) are consistent with these dependencies.

The efficiency with which MBZ can inhibit the formation of the primary cilium suggests that this anti-Hh effect might account for much of its activity against brain tumors and other tumor types thus far tested. Effects on other targets may also be relevant. For example, signals arising from WNT and PDGF ligands travel through the primary cilium (3). However, the developmental abnormalities that arise in mutant mice deficient for ciliogenesis most clearly overlap with those caused by Hh signaling defects (3). Beyond the primary cilium, microtubule assembly plays a fundamental role in cell division. Our results cannot rule out effects of MBZ on the mitotic spindle as a cause of cytotoxicity. However, this type of antiproliferative activity would not be highly specific for cancer cells. Indeed, mitotic spindle checkpoint defects that are found in many cancers have been proposed to confer relative resistance to microtubule inhibitors (54). Interestingly, MBZ-treated xenografts have been found to exhibit reduced vascularity (17). VEGF-A has accordingly

been proposed as a target of benzimidazole therapy (18). Inhibition of Hh activation potently stimulates angiogenesis by the paracrine induction of VEGF-A and other angiogenic factors (55), and could therefore account for these seemingly disparate observations.

The central role of the primary cilium in Hh pathway activation suggests that interfering with cilia formation should be an effective strategy for targeting Hh-driven tumors. The inhibitory effect of microtubule inhibitors on Hh signaling has been demonstrated by unbiased screens that have identified such agents indirectly, as inhibitors of GLI activity, or by direct inhibition of cilia formation and function (33,56,57). Thus far, the anti-microtubule agents identified in these screens are either highly toxic, or at early stages of characterization. Our data suggest that MBZ might represent a simple path forward for this promising therapeutic strategy.

A burgeoning body of evidence suggests that Hh signaling is involved in the initiation and/or maintenance of a large proportion of human cancers (2,5,6,29). The repurposing of MBZ as an anticancer therapeutic will be guided by our rapidly growing understanding of the Hh pathway and how it contributes to tumor growth. It will be important to understand how MBZ interacts with other agents, including other Hedgehog inhibitors. In particular, the additive effect of MBZ on vismodegib that we observed *in vitro* suggests a combinatorial strategy that could potentially alleviate the untoward effects associated with vismodegib and also suppress recurrence. Clinical trials will be the next step in exploring these new possibilities.

Supplementary Material

Refer to Web version on PubMed Central for supplementary material.

Acknowledgments

Financial support: This study was funded by grant R01CA157535 from the National Cancer Institute to F. Bunz. R-Y. Bai, A. Borodovsky and G.J. Riggins were supported by the Virginia and D.K. Ludwig Fund for Cancer Research. J.H.Chung was supported by the AACR-Fight Colorectal Cancer Fellowship. G.J. Riggins is supported by the Irving Sherman Professorship. The Johns Hopkins research core facilities were funded in part by Cancer Center grant P30CA006973 from the National Cancer Institute.

The authors thank Dr. Verena Staedke for advice regarding the animal experiments.

Abbreviations

MBZ	mebendazole
Hh	hedgehog
FBS	fetal bovine serum

References

1. Yang L, Xie G, Fan Q, Xie J. Activation of the hedgehog-signaling pathway in human cancer and the clinical implications. Oncogene. 2010; 29:469–81. [PubMed: 19935712]
2. Barakat MT, Humke EW, Scott MP. Learning from Jekyll to control Hyde: Hedgehog signaling in development and cancer. Trends Mol Med. 2010; 16:337–48. [PubMed: 20696410]

3. Goetz SC, Anderson KV. The primary cilium: a signalling centre during vertebrate development. Nat Rev Genet. 2010; 11:331–44. [PubMed: 20395968]

4. Corbit KC, Aanstad P, Singla V, Norman AR, Stainier DY, Reiter JF. Vertebrate Smoothened functions at the primary cilium. Nature. 2005; 437:1018–21. [PubMed: 16136078]

5. Berman DM, Karhadkar SS, Maitra A, Montes De Oca R, Gerstenblith MR, Briggs K, et al. Widespread requirement for Hedgehog ligand stimulation in growth of digestive tract tumours. Nature. 2003; 425:846–51. [PubMed: 14520411]

6. Yauch RL, Gould SE, Scales SJ, Tang T, Tian H, Ahn CP, et al. A paracrine requirement for hedgehog signalling in cancer. Nature. 2008; 455:406–10. [PubMed: 18754008]

7. Amakye D, Jagani Z, Dorsch M. Unraveling the therapeutic potential of the Hedgehog pathway in cancer. Nat Med. 2013; 19:1410–22. [PubMed: 24202394]

8. Low JA, de Sauvage FJ. Clinical experience with Hedgehog pathway inhibitors. J Clin Oncol. 2010; 28:5321–26. [PubMed: 21041712]

9. LoRusso PM, Rudin CM, Reddy JC, Tibes R, Weiss GJ, Borad MJ, et al. Phase I trial of hedgehog pathway inhibitor vismodegib (GDC-0449) in patients with refractory, locally advanced or metastatic solid tumors. Clin Cancer Res. 2011; 17:2502–11. [PubMed: 21300762]

10. Von Hoff DD, LoRusso PM, Rudin CM, Reddy JC, Yauch RL, Tibes R, et al. Inhibition of the hedgehog pathway in advanced basal-cell carcinoma. N Engl J Med. 2009; 361:1164–72. [PubMed: 19726763]

11. Berlin J, Bendell JC, Hart LL, Firdaus I, Gore I, Hermann RC, et al. A randomized phase II trial of vismodegib versus placebo with FOLFOX or FOLFIRI and bevacizumab in patients with previously untreated metastatic colorectal cancer. Clin Cancer Res. 2013; 19:258–67. [PubMed: 23082002]

12. Rudin CM, Hann CL, Laterra J, Yauch RL, Callahan CA, Fu L, et al. Treatment of medulloblastoma with hedgehog pathway inhibitor GDC-0449. N Engl J Med. 2009; 361:1173–78. [PubMed: 19726761]

13. Yauch RL, Dijkgraaf GJ, Alicke B, Januario T, Ahn CP, Holcomb T, et al. Smoothened mutation confers resistance to a Hedgehog pathway inhibitor in medulloblastoma. Science. 2009; 326:572–74. [PubMed: 19726788]

14. Kim J, Aftab BT, Tang JY, Kim D, Lee AH, Rezaee M, et al. Itraconazole and arsenic trioxide inhibit Hedgehog pathway activation and tumor growth associated with acquired resistance to smoothened antagonists. Cancer Cell. 2013; 23:23–34. [PubMed: 23291299]

15. Martarelli D, Pompei P, Baldi C, Mazzoni G. Mebendazole inhibits growth of human adrenocortical carcinoma cell lines implanted in nude mice. Cancer Chemother Pharmacol. 2008; 61:809–17. [PubMed: 17581752]

16. Sasaki J, Ramesh R, Chada S, Gomyo Y, Roth JA, Mukhopadhyay T. The anthelmintic drug mebendazole induces mitotic arrest and apoptosis by depolymerizing tubulin in non-small cell lung cancer cells. Mol Cancer Ther. 2002; 1:1201–9. [PubMed: 12479701]

17. Mukhopadhyay T, Sasaki J, Ramesh R, Roth JA. Mebendazole elicits a potent antitumor effect on human cancer cell lines both in vitro and in vivo. Clin Cancer Res. 2002; 8:2963–9. [PubMed: 12231542]

18. Pourgholami MH, Yan Cai Z, Lu Y, Wang L, Morris DL. Albendazole: a potent inhibitor of vascular endothelial growth factor and malignant ascites formation in OVCAR-3 tumor-bearing nude mice. Clin Cancer Res. 2006; 12:1928–35. [PubMed: 16551879]

19. Doudican N, Rodriguez A, Osman I, Orlow SJ. Mebendazole induces apoptosis via Bcl-2 inactivation in chemoresistant melanoma cells. Mol Cancer Res. 2008; 6:1308–15. [PubMed: 18667591]

20. Nygren P, Fryknas M, Agerup B, Larsson R. Repositioning of the anthelmintic drug mebendazole for the treatment for colon cancer. J Cancer Res Clin Oncol. 2013; 139:2133–40. [PubMed: 24135855]

21. Dobrosotskaya IY, Hammer GD, Schteingart DE, Maturen KE, Worden FP. Mebendazole monotherapy and long-term disease control in metastatic adrenocortical carcinoma. Endocr Pract. 2011; 17:e59–62. [PubMed: 21454232]

22. Nygren P, Larsson R. Drug repositioning from bench to bedside: Tumour remission by the antihelmintic drug mebendazole in refractory metastatic colon cancer. Acta Oncol. 2014; 53:427–8. [PubMed: 24160353]
23. Bai RY, Staedtke V, Aprhys CM, Gallia GL, Riggins GJ. Antiparasitic mebendazole shows survival benefit in 2 preclinical models of glioblastoma multiforme. Neuro Oncol. 2011; 13:974–982. [PubMed: 21764822]
24. Russell GJ, Gill JH, Lacey E. Binding of [3H]benzimidazole carbamates to mammalian brain tubulin and the mechanism of selective toxicity of the benzimidazole anthelmintics. Biochem Pharmacol. 1992; 43:1095–100. [PubMed: 1554382]
25. Kohler P, Bachmann R. Intestinal tubulin as possible target for the chemotherapeutic action of mebendazole in parasitic nematodes. Mol Biochem Parasitol. 1981; 4:325–36. [PubMed: 7335116]
26. El-On J. Benzimidazole treatment of cystic echinococcosis. Acta Trop. 2003; 85:243–52. [PubMed: 12606103]
27. Monje M, Mitra SS, Freret ME, Raveh TB, Kim J, Masek M, et al. Hedgehog-responsive candidate cell of origin for diffuse intrinsic pontine glioma. Proc Natl Acad Sci USA. 2011; 108:4453–58. [PubMed: 21368213]
28. Gruber Filbin M, Dabral SK, Pazyra-Murphy MF, Ramkissoon S, Kung AL, Pak E, et al. Coordinate activation of Shh and PI3K signaling in PTEN-deficient glioblastoma: new therapeutic opportunities. Nat Med. 2013; 19:1518–23. [PubMed: 24076665]
29. Watkins DN, Berman DM, Burkholder SG, Wang B, Beachy PA, Baylin SB. Hedgehog signalling within airway epithelial progenitors and in small-cell lung cancer. Nature. 2003; 422:313–17. [PubMed: 12629553]
30. Stecca B, Mas C, Clement V, Zbinden M, Correa R, Piguet V, et al. Melanomas require HEDGEHOG-GLI signaling regulated by interactions between GLI1 and the RAS-MEK/AKT pathways. Proc Natl Acad Sci USA. 2007; 104:5895–900. [PubMed: 17392427]
31. Bhattacharya R, Kwon J, Ali B, Wang E, Patra S, Shridhar V, et al. Role of hedgehog signaling in ovarian cancer. Clin Cancer Res. 2008; 14:7659–66. [PubMed: 19047091]
32. Simon DP, Hammer GD. Adrenocortical stem and progenitor cells: implications for adrenocortical carcinoma. Mol Cell Endocrinol. 2012; 351:2–11. [PubMed: 22266195]
33. Kim J, Tang JY, Gong R, Kim J, Lee JJ, Clemons KV, et al. Itraconazole, a commonly used antifungal that inhibits Hedgehog pathway activity and cancer growth. Cancer Cell. 2010; 17:388–99. [PubMed: 20385363]
34. Taipale J, Chen JK, Cooper MK, Wang B, Mann RK, Milenkovic L, et al. Effects of oncogenic mutations in Smoothened and Patched can be reversed by cyclopamine. Nature. 2000; 406:1005–9. [PubMed: 10984056]
35. Low WC, Wang C, Pan Y, Huang XY, Chen JK, Wang B. The decoupling of Smoothened from Galphai proteins has little effect on Gli3 protein processing and Hedgehog-regulated chick neural tube patterning. Dev Biol. 2008; 321:188–96. [PubMed: 18590719]
36. Roessler E, Ermilov AN, Grange DK, Wang A, Grachtchouk M, Dlugosz AA, et al. A previously unidentified amino-terminal domain regulates transcriptional activity of wild-type and disease-associated human GLI2. Hum Mol Genet. 2005; 14:2181–88. [PubMed: 15994174]
37. Sharma N, Kosan ZA, Stallworth JE, Berbari NF, Yoder BK. Soluble levels of cytosolic tubulin regulate ciliary length control. Mol Biol Cell. 2011; 22:806–816. [PubMed: 21270438]
38. Jin H, White SR, Shida T, Schulz S, Aguiar M, Gygi SP, et al. The conserved Bardet-Biedl syndrome proteins assemble a coat that traffics membrane proteins to cilia. Cell. 2010; 141:1208–19. [PubMed: 20603001]
39. Jacobs VL, Valdes PA, Hickey WF, De Leo JA. Current review of in vivo GBM rodent models: emphasis on the CNS-1 tumour model. ASN Neuro. 2011; 3:e00063. [PubMed: 21740400]
40. Triscott J, Lee C, Foster C, Manoranjan B, Pambid MR, Berns R, et al. Personalizing the Treatment of Pediatric Medulloblastoma: Polo-like Kinase 1 as a Molecular Target in High-Risk Children. Cancer Res. 2013; 73:6734–44. [PubMed: 24019381]
41. Northcott PA, Korshunov A, Pfister SM, Taylor MD. The clinical implications of medulloblastoma subgroups. Nat Rev Neurol. 2012; 8:340–51. [PubMed: 22565209]

42. Martinelli DC, Fan CM. Gas1 extends the range of Hedgehog action by facilitating its signaling. Genes Dev. 2007; 21:1231–43. [PubMed: 17504940]
43. Kola I, Landis J. Can the pharmaceutical industry reduce attrition rates? Nat Rev Drug Discov. 2004; 3:711–715. [PubMed: 15286737]
44. Huang R, Southall N, Wang Y, Yasgar A, Shinn P, Jadhav A, et al. The NCGC pharmaceutical collection: a comprehensive resource of clinically approved drugs enabling repurposing and chemical genomics. Sci Transl Med. 2011; 3:80ps16.
45. Smoll NR, Drummond KJ. The incidence of medulloblastomas and primitive neurectodermal tumours in adults and children. J Clin Neurosci. 2012; 19:1541–4. [PubMed: 22981874]
46. de Silva NR, Sirisena JL, Gunasekera DP, Ismail MM, de Silva HJ. Effect of mebendazole therapy during pregnancy on birth outcome. Lancet. 1999; 353:1145–9. [PubMed: 10209979]
47. Braithwaite PA, Roberts MS, Allan RJ, Watson TR. Clinical pharmacokinetics of high dose mebendazole in patients treated for cystic hydatid disease. Eur J Clin Pharmacol. 1982; 22:161–9. [PubMed: 7094986]
48. Bryceson AD, Woestenborghs R, Michiels M, van den Bossche H. Bioavailability and tolerability of mebendazole in patients with inoperable hydatid disease. Trans R Soc Trop Med Hyg. 1982; 76:563–4. [PubMed: 6926777]
49. Bekhti A. Serum concentrations of mebendazole in patients with hydatid disease. Int J Clin Pharmacol Ther Toxicol. 1985; 23:633–41. [PubMed: 4093204]
50. Levin MH, Weinstein RA, Axelrod JL, Schantz PM. Severe, reversible neutropenia during high-dose mebendazole therapy for echinococcosis. JAMA. 1983; 249:2929–31. [PubMed: 6842806]
51. Rohatgi R, Milenkovic L, Scott MP. Patched1 regulates hedgehog signaling at the primary cilium. Science. 2007; 317:372–6. [PubMed: 17641202]
52. Huangfu D, Anderson KV. Cilia and Hedgehog responsiveness in the mouse. Proc Natl Acad Sci USA. 2005; 102:11325–30. [PubMed: 16061793]
53. Barakat MT, Humke EW, Scott MP. Kif3a is necessary for initiation and maintenance of medulloblastoma. Carcinogenesis. 2013; 34:1382–92. [PubMed: 23389290]
54. Weaver BA, Cleveland DW. Decoding the links between mitosis, cancer, and chemotherapy: The mitotic checkpoint, adaptation, and cell death. Cancer Cell. 2005; 8:7–12. [PubMed: 16023594]
55. Chen W, Tang T, Eastham-Anderson J, Dunlap D, Alicke B, Nannini M, et al. Canonical hedgehog signaling augments tumor angiogenesis by induction of VEGF-A in stromal perivascular cells. Proc Natl Acad Sci USA. 2011; 108:9589–94. [PubMed: 21597001]
56. Hyman JM, Firestone AJ, Heine VM, Zhao Y, Ocasio CA, Han K, et al. Small-molecule inhibitors reveal multiple strategies for Hedgehog pathway blockade. Proc Natl Acad Sci USA. 2009; 106:14132–7. [PubMed: 19666565]
57. Wu VM, Chen SC, Arkin MR, Reiter JF. Small molecule inhibitors of Smoothened ciliary localization and ciliogenesis. Proc Natl Acad Sci USA. 2012; 109:13644–9. [PubMed: 22864913]

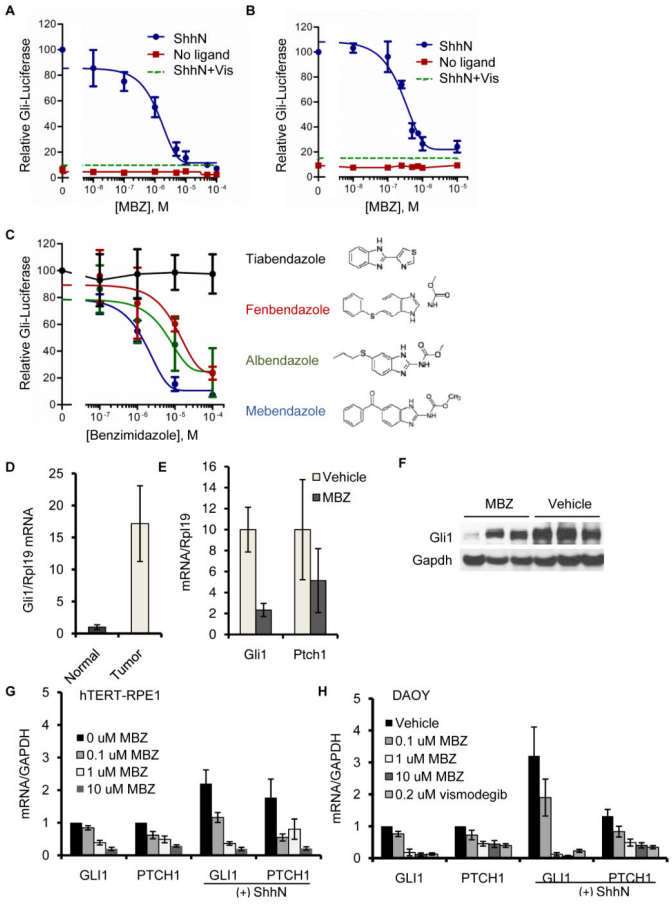

Figure 1.

MBZ inhibits Hh signaling. (A) Shh-Light II cells maintained in low serum conditions were incubated in ShhN-conditioned medium or control medium, in the presence of MBZ at the indicated concentrations. The activity of the stably integrated Gli-luc reporter was measured after 48 h of treatment. The effect on this assay of 0.2 μM vismodegib (Vis) is indicated by the dashed line. (B) C3H10T1/2 mouse fibroblasts were co-transfected with the Gli-luc and *renilla* luciferase reporters. After 24 h, MBZ was added for an additional 48h in low serum media prior to cell lysis and measurement of luciferase activity. The effect of 0.2 μM vismodegib (Vis) is indicated by the dashed line. (C) The effect of MBZ on Gli-luc reporter activity in Shh-Light2 cells was compared with that of the structurally related benzamidizoles albendazole, fenbendazole, and tiabendazole. Treatment times and conditions were as in (A). (D) Endogenous levels of *Gli1* transcripts in syngeneic, GL261 gliomas and in normal brain tissue from the contralateral region were measured by qRT-PCR. (E) *Gli1* expression was measured by qRT-PCR in untreated and MBZ-treated GL261 tumors. Each measurement was standardized to a parallel measurement from a contralateral brain section that did not contain tumor tissue. (F) Relative protein levels of *Gli1* in three untreated and three MBZ-treated GL261 tumors were assessed by immunoblot. (G) Immortalized hTERT-RPE1 cells or DAOY medulloblastoma cells (H) growing in low serum were treated with ShhN-conditioned or control medium for 48 h. MBZ was included

during this treatment period at the concentrations indicated. *GLI1* and *PTCH1* transcript levels were assessed by qRT-PCR.

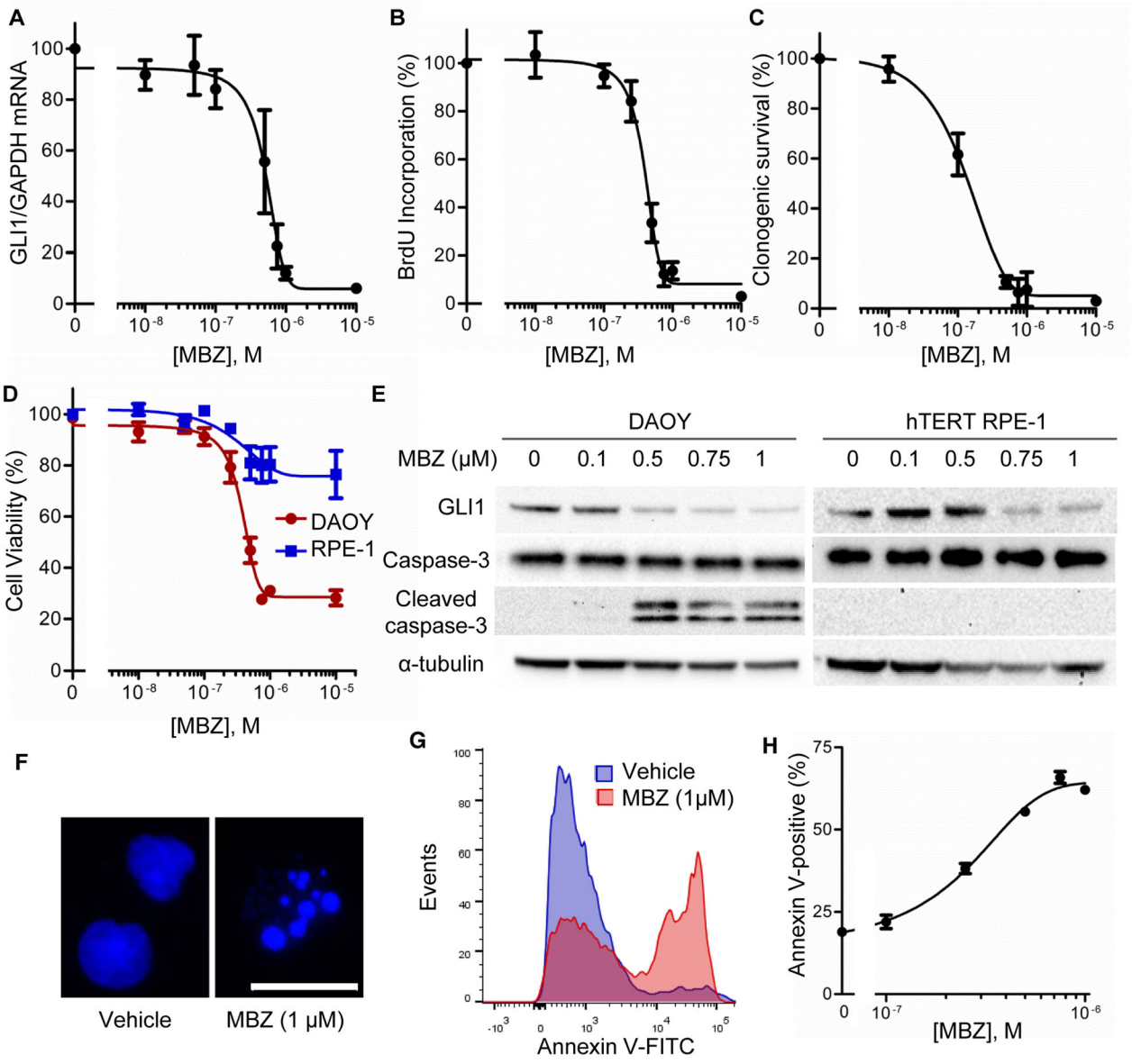

Figure 2.

Effect of MBZ on Hh-signaling, growth and survival of Hh-dependent medulloblastoma cells. Subconfluent DAOY cultures maintained under low serum conditions were treated for 48 h with MBZ at varying concentrations. (A) *GLI1* expression was assayed by qRT-PCR. (B) Cell proliferation was assessed by measuring the incorporation of BrdU over 2 h. (C) Cell survival was quantified by a clonogenic assay. (D) The effect of MBZ on cell viability was comparatively assessed by CellTiter-Blue in hTERT-RPE1 (blue) and DAOY (red). (E) The expression of GLI1 protein and cleavage of caspase-3 were assessed by immunoblot in DAOY and hTERT-RPE1 cells treated with MBZ for 12 h, under low serum conditions. α-tubulin was probed as a loading control. (F) Representative nuclei from MBZ-treated DAOY cells and untreated controls, stained with Hoechst 33258. Scale bar, 20 μm. (G) Annexin V stained cells were quantified by flow cytometry, after 24 h of MBZ treatment (1 μM) under

low serum conditions. (H) The proportion of Annexin V positive cells after treatment with various concentrations of MBZ, as in (G).

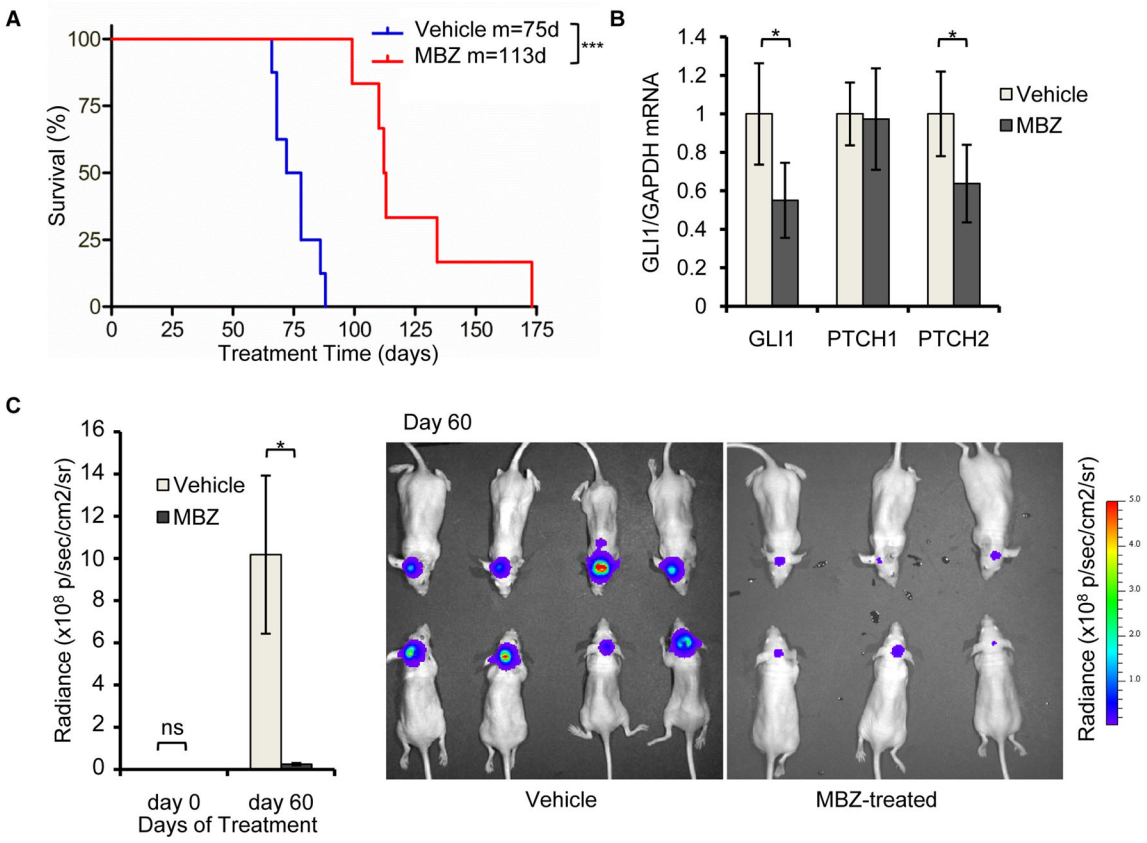

Figure 3.

MBZ suppresses the growth of medulloblastoma cells and Hh signaling *in vivo*. DAOY cells expressing firefly luciferase were grown as orthotopic xenograft tumors following injection into the cerebella of nude mice. After 5 d, mice were treated with 50 mg/kg MBZ (n=6) or mock-treated (Vehicle; n=8). (A) Survival of mice with DAOY cell-derived orthotopic tumors. Median survival was 75 d in the control (Vehicle) group and 113 d in the MBZ-treated group (p=0.001). One MBZ-treated mouse was euthanized after surviving six months without presenting any symptoms of lethal tumor growth. (B) Total RNA was harvested from representative tumors at the time of death. *GLI1*, *PTCH1 and PTCH2* transcripts were quantified by qRT-PCR. (C) Tumor growth in live animals was quantified by bioluminescence imaging 5 d after implantation and again following 60 d of treatment. Representative images from the 60 d time point are shown at right.

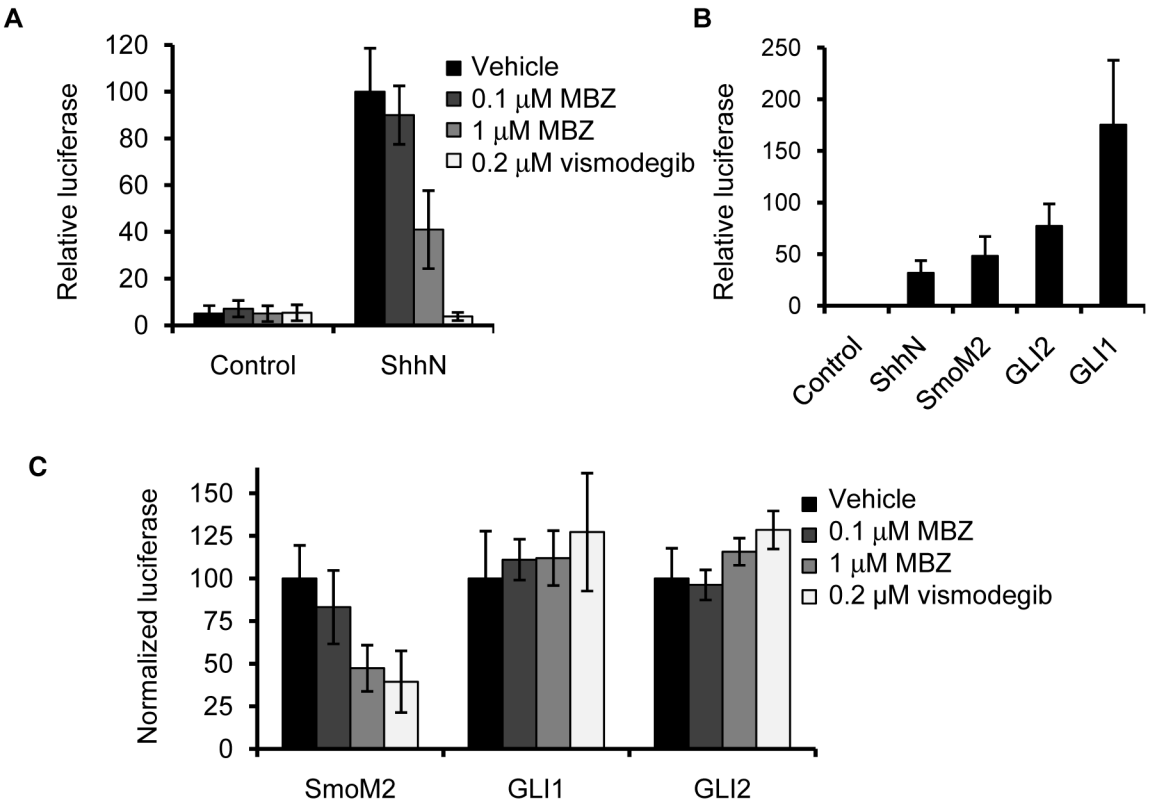

Figure 4.

MBZ inhibits activation of SMO. (A) NIH3T3 fibroblasts co-transfected with Gli-luc and *renilla* reporter plasmids were maintained in low serum conditions for 48 h in the presence of ShhN-conditioned or control media. During this period, MBZ or vismodegib were added at the indicated concentrations. (B) A direct comparison of Gli-luc activation in NIH3T3 cells 48 h after treatment with ShhN ligand, or 72 h after cotransfection with plasmids that drive exogenous expression of the Ptch1-resistant Smo mutant SmoM2, GLI1 or GLI2 in low serum media. (C) MBZ or vismodegib was added to SmoM2-, GLI1-, or GLI2-transfected NIH3T3 cells during 48 h of incubation in low serum conditions. The activation of a co-transfected Gli-luc reporter by each overexpressed gene, in the absence of drug treatment, was normalized to 100.

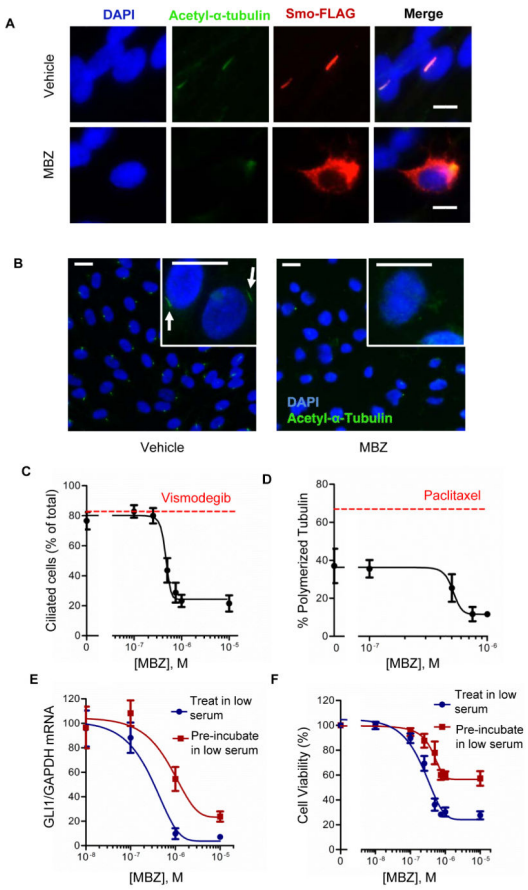

Figure 5.

MBZ inhibits formation of primary cilia. (A) A Smo-FLAG fusion protein was expressed in hTERT-RPE1 cells by transient transfection. After 48 h incubation in low serum and treatment with 1 uM MBZ or vehicle, cells were fixed, permeabilized and stained with antibodies directed against acetyl-α-tubulin (green) and FLAG (red). Nuclei were counterstained with DAPI. Scale bar, 10 μm. (B) Cilia were numerically assessed by acetyl-α-tubulin staining in hTERT-RPE1 cells maintained in low serum conditions and treated with MBZ. Primary cilia (indicated by arrows) could be visualized on individual cells (inset). Scale bar, 20 μm. (C) The effects of MBZ or 0.2 μM vismodegib (red line) on the proportion of ciliated cells. (D) hTERT-RPE1 cells were treated with MBZ at the indicated concentrations or with 10 nM paclitaxel (red line) for 48 h under low serum conditions. Polymerized and unpolymerized tubulin fractions were quantified by immunobloting, normalized to the loading control β-actin, and expressed as the proportion of polymerized tubulin compared to the combined polymerized and unpolymerized tubulin. (E) *GLI1* expression was assessed in DAOY cells that were incubated with MBZ for 48 h under the low serum conditions that allow formation of the primary cilium (“Treat in low serum”), or that were first maintained in low serum for 20 h prior to before adding MBZ for an additional 48 h (“Pre-incubate in low serum”). (F) Cell viability was assessed by CellTiter-Blue after the treatments described in (E).

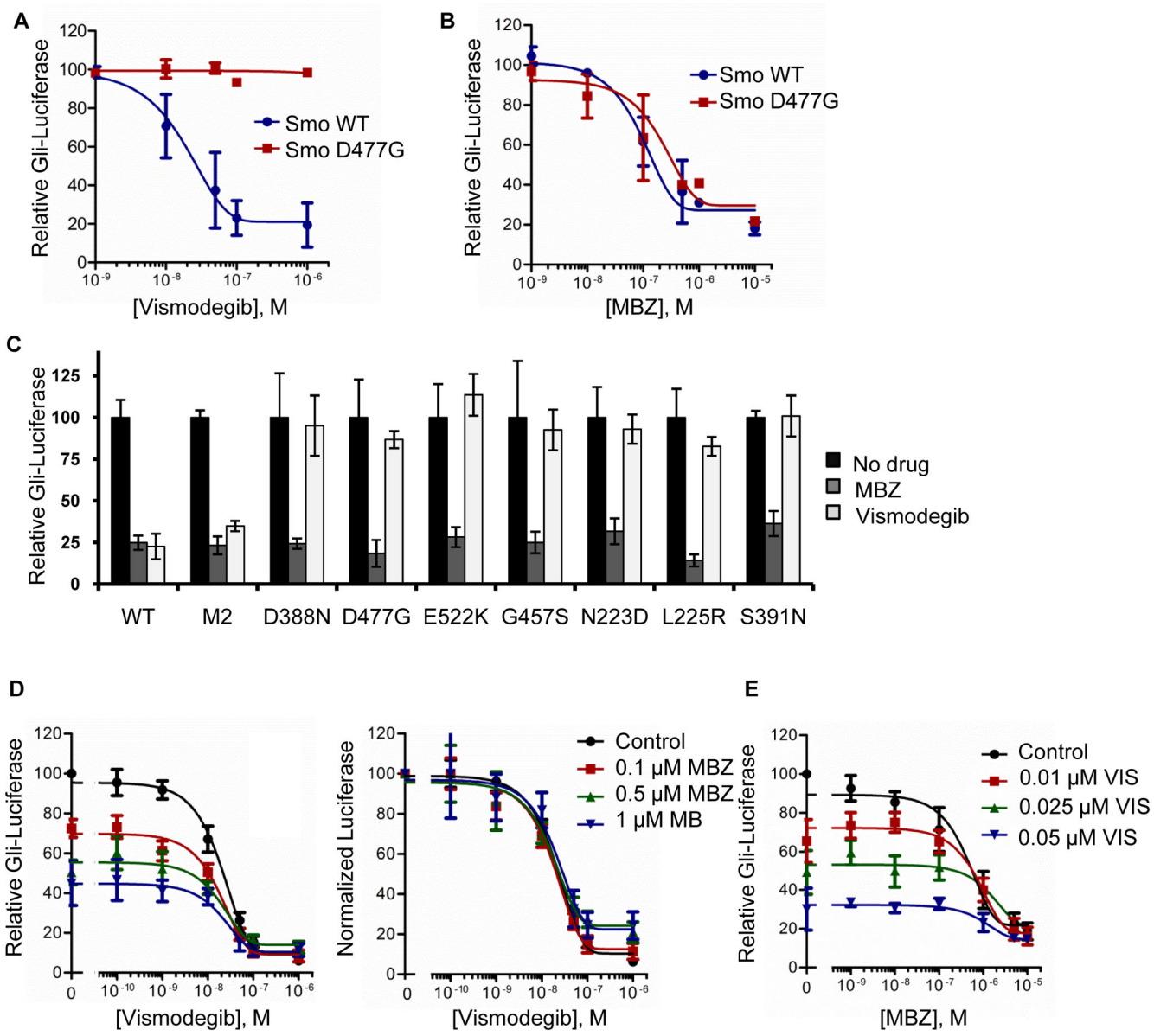

Figure 6.

Additive effects of MBZ and vismodegib against SMO signaling. Wild type *Smo* or the *Smo* D477G mutant were expressed with the Gli-luc and *renilla* luciferase reporters by co-transfection into *Smo*−/− MEFs. After 24 h, cells were treated with (A) vismodegib or (B) MBZ at the indicated concentrations, in the presence of ShhN-conditioned medium. (C) The effects of 1 μM MBZ and 0.2 μM vismodegib on Smo-dependent activation of the Gli-luc reporter were assessed against an expanded panel of *Smo* mutants. WT, wild type *Smo*. (D) The combined effects of vismodegib and MBZ on relative Gli-luc activity were tested in Shh Light2 cells under low serum conditions with supplemental ShhN-media. The relative luciferase readout was normalized to 100 for each MBZ concentration, so that the curves could be superimposed. The IC_{50} of vismodegib was unchanged by addition of MBZ. (E) A

modification of the experiment shown in D, in which MBZ was titrated into the Shh Light2 Gli-luc assay along with fixed concentrations of vismodegib.